electronics

MDPI

Article

Research on Optimal Scheduling of the Combined Cooling, Heating, and Power Microgrid Based on Improved Gold Rush Optimization Algorithm

Wei Liu, Zhenhai Dou *, Yi Yan, Tong Zhou and Jiajia Chen

School of Electrical and Electronic Engineering, Shandong University of Technology, Zibo 255000, China; 23504040579@stumail.sdut.edu.cn (W.L.); 23504040588@stumail.sdut.edu.cn (Y.Y.); 18560907312@163.com (T.Z.); jjchen@sdut.edu.cn (J.C.)

* Correspondence: douzhenhai@sdut.edu.cn

Abstract

To address the shortcomings of poor convergence and the ease of falling into local optima when using the traditional gold rush optimization (GRO) algorithm to solve the complex scheduling problem of a combined cooling, heating, and power (CCHP) microgrid system, an optimal scheduling model for a microgrid based on the improved gold rush optimization (IGRO) algorithm is proposed. First, the Halton sequence is introduced to initialize the population, ensuring a uniform and diverse distribution of prospectors, which enhances the algorithm's global exploration capability. Then, a dynamically adaptive weighting factor is applied during the gold mining phase, enabling the algorithm to adjust its strategy across different search stages by balancing global exploration and local exploitation, thereby improving the convergence efficiency of the algorithm. In addition, a weighted global optimal solution update strategy is employed during the cooperation phase, enhancing the algorithm's global search capability while reducing the risk of falling into local optima by adjusting the balance of influence between the global best solution and local agents. Finally, a *t*-distribution mutation strategy is introduced to improve the algorithm's local search capability and convergence speed. The IGRO algorithm is then applied to solve the microgrid scheduling problem, with the objective function incorporating power purchase and sale cost, fuel cost, maintenance cost, and environmental cost. The example results show that, compared with the GRO algorithm, the IGRO algorithm reduces the average total operating cost of the microgrid by 3.29%, and it achieves varying degrees of cost reduction compared to four other algorithms, thereby enhancing the system's economic benefits.

Keywords: improved gold rush optimization algorithm; combined cooling; heating and power system; microgrid; optimization scheduling; Halton sequence; *t*-distribution mutation

Academic Editor: Jianguo Zhu

Received: 9 July 2025
Revised: 2 August 2025
Accepted: 5 August 2025
Published: 6 August 2025

Citation: Liu, W.; Dou, Z.; Yan, Y.; Zhou, T.; Chen, J. Research on Optimal Scheduling of the Combined Cooling, Heating, and Power Microgrid Based on Improved Gold Rush Optimization Algorithm. *Electronics* **2025**, *14*, 3135. https://doi.org/10.3390/electronics14153135

1. Introduction

Over the past few years, with the increasing problems of fossil energy depletion and environmental degradation, the survival and development of human beings have come to face great challenges [1–3]. Conventional energy systems employ a singular energy management strategy, which hampers the realization of the synergistic and complementary benefits of diverse energy sources, thereby constraining enhancements in energy efficiency, conservation, and emissions reduction, while also impeding the development and utilization potential of renewable energy sources to some degree [4–6]. Microgrids, as a flexible and efficient energy distribution and management scheme, have received widespread

attention, especially combined cooling, heating, and power microgrids, which can produce electricity while using the waste heat from gas turbines for heating or cooling. This allows for gradient energy utilization, with the energy utilization efficiency reaching 70% to 90%, which has significant benefits for energy conservation and protection of the environment, as well as effectively reducing the operating pressure of the power grid [7–9]. The national electric power industry is actively promoting the efficient coupling and utilization of energy in order to achieve the lowest operating costs and optimal environmental benefits, further reduce the costs of electricity for consumers, and enhance system stability. However, high-dimensional random variables and large-scale optimization problems in microgrids pose significant challenges in scheduling [10]. Therefore, the optimal scheduling of microgrids is of great significance [11–13].

For the complex optimization problems that are faced in practical engineering, especially in situations with multiple objectives, constraints, and high uncertainty, existing optimization methods often struggle to fulfill the demands of high effectiveness, accuracy, and operability in practical applications. Optimization problems in engineering typically involve large-scale data processing, dynamically changing system environments, and diversified objectives and constraints, and traditional optimization algorithms can encounter many challenges when solving these problems, such as high computational complexity, slow convergence, and poor stability. In order to overcome these problems, an increasing amount of research is focusing on improving algorithms. Ref. [14] introduced a variable inertia weight into the whale optimization algorithm to balance global exploration and local exploitation. Ref. [15] introduced an adaptive displacement strategy, which emphasizes the role of the optimal individual to improve the balance of local and global search in the grey wolf optimization algorithm, thereby enhancing the accuracy of fault diagnosis for power transformers. Ref. [16] proposed a dual stochastic perturbation strategy in the gorilla algorithm, which mitigates the swarming effect of gorillas and improves the algorithm's capacity to avoid becoming trapped in local optima. Ref. [17] combined the sparrow search algorithm's explorer and joiner methods with the butterfly optimization algorithm, dividing the butterfly population into two sub-groups of varying sizes and improving the algorithm's global exploration capability. Ref. [18] employed a horizontal crossover strategy in the honey badger algorithm to generate new solutions, thereby enhancing the search capability of the algorithm. According to the trial results, the enhanced algorithm not only reduces operational costs, but also significantly reduces the energy waste rate. Ref. [19] proposed an improved mayfly algorithm for parameter identification of permanent magnet synchronous motors, which enhances population diversity through SPM chaotic mapping, improves global search ability by employing Cauchy and Gaussian mutations based on individual fitness, and strengthens the ability to escape local optima using a chaotic refractive reverse learning strategy, thereby significantly improving the accuracy of parameter identification. With the continuous development of intelligent optimization algorithms, an increasing number of novel algorithms have demonstrated strong adaptability and competitiveness in solving complex engineering problems. Compared to traditional optimization methods, these improved intelligent algorithms can not only cope more effectively with the challenges of complex problems, such as high-dimensional, multi-peaked, and non-linear problems, but also offer significant advantages with regard to global search capability, convergence rate, and computational efficiency.

With the advancement of intelligent algorithms, novel approaches have demonstrated superior performance in optimizing distributed energy resource configurations, not only reducing operational costs, but also enabling more environmentally sustainable dispatch strategies. Currently, the majority of researchers, both domestically and internationally, address the problem of optimal scheduling of microgrids by formulating objective func-

tions and defining corresponding constraints, and employing intelligent optimization algorithms to obtain effective solutions [20]. Ref. [21] employed a butterfly optimization algorithm to assess a CCHP system's energy efficiency and pollutant emissions. Ref. [22] proposed a hybrid optimization strategy that integrated a Tent map-based chaotic search mechanism with a non-linear adaptive particle swarm optimization algorithm to solve the CCHP system's complex multi-energy coupling features, thereby improving its economic performance. Ref. [23] introduced a rank pair learning-based crisscross optimization algorithm to determine the most suitable output of distributed power units in microgrids. The study showed that the algorithm exhibits desirable global convergence properties and significantly reduces the operational costs of the microgrid. Ref. [24] proposed an improved multi-objective multi-verse optimization algorithm by incorporating a mechanism based on opposition learning, a mechanism for dominance ranking, a population-guidance mechanism, and a seagull attack operator, thereby enhancing its capability for optimizing the CCHP system's configuration using various methods. Ref. [25] significantly enhances the artificial bee colony algorithm's ability for broad exploration and precise local exploitation by introducing a global best-guided strategy and a dynamic step-size adjustment mechanism, thereby effectively reducing the operational cost of the system. Ref. [26] incorporated a sinusoidal chaotic map, a shared factor mechanism, and a random walk strategy into the sparrow search algorithm. The improved sparrow search algorithm not only promotes a more even distribution of the initial population, but also boosts information sharing among individuals and enhances exploration capability during the local search phase. The fusion of these strategies greatly strengthens the algorithm's capacity to dynamically balance local exploitation and global exploration, thereby effectively lowering the total operational cost of the microgrid. Ref. [27] proposed a planetary search algorithm to analyze the energy utilization performance of a CCHP system under time-sharing economic operation. Ref. [28] introduced a chaotic mapping approach based on circle mapping and applied it to initialize the northern goshawk optimization algorithm. The sequence exhibits higher complexity and stronger randomness, which improves the problem of premature convergence in the algorithm, thereby significantly enhancing the operational performance of the microgrid system. Ref. [29] proposed an improved mother optimization algorithm that dynamically adjusts both the population size and parameter configurations in response to the problem's characteristics and the evolving state of the optimization process. By integrating an adaptive control mechanism, the algorithm effectively accommodates dynamic environmental variations, preserves population variety, and reduces the likelihood of early convergence. As a result, the algorithm achieves an effective balance between local and global exploration. In microgrid scheduling applications, the proposed method significantly reduces system energy consumption and demonstrates promising performance in mitigating carbon dioxide emissions. Ref. [30] introduced the spiral position update strategy, dynamic weight factor, Levy flight strategy, and t-distribution mutation strategy into the dung beetle optimizer algorithm, which, together, help to effectively prevent premature convergence of particles caused by them becoming trapped in local optima. Ref. [31] introduced an improved honey badger algorithm that combined a variable spiral factor with a linear parameter-decreasing strategy, thereby effectively reducing the tendency of the algorithm to become trapped in local optima. The experimental results showed that the improved honey badger algorithm significantly increases the economic advantages of the microgrid.

There have been many studies on the gold rush algorithm [32], which have deeply analyzed and improved it in various aspects. Ref. [33] employed a migration strategy in combination with the Levy flight mechanism and joining of a follower group, thereby enhancing the breadth and flexibility of the fusion search approach. Subsequently, a dynamic opposite learning approach was used to increase population diversity during the

panning phase. Moreover, a cooperative strategy involving multiple agents was introduced to strengthen the algorithm's search capability in the collaboration stage. Finally, the random differential mutation method was applied to enable the algorithm to escape local optima. The algorithm enhances the overall network coverage while simultaneously minimizing redundant nodes and lowering energy usage. Ref. [34] first introduced a good point-set population initialization to enhance the global exploration capabilities of the GRO algorithm. Second, the dynamic Levy flight search approach was applied to enhance the algorithm's population diversity. Then, a dynamic centroid reverse learning technique was introduced to update the agents within the group, thereby improving the overall quality of the population. Finally, a dynamic tangent flight was used to maintain population diversity, which helps the algorithm to avoid entrapment in local optima. The algorithm provides a better path planning scheme for the problem of 3D unmanned aircraft route planning. Ref. [35] used quasi-reverse learning to initialize the population, replaced the original convergence factor with the sigmoid function, and incorporated the golden sine algorithm to enhance optimization performance. The improved GRO algorithm exhibits lower maximum and average reflection coefficients compared to the GRO algorithm in the design optimization of multilayer microwave absorbers under normal incidence. The above mentioned literature has improved the GRO algorithm and applied it to different engineering fields. However, no research has yet been carried out on solving the problem of optimal scheduling of a CCHP microgrid using the GRO algorithm.

The GRO algorithm features a remarkable adaptive search mechanism and exhibits strong adaptability in addressing the integrated requirements of robustness, real-time performance, and scalability in optimal microgrid scheduling. In addition, the GRO algorithm does not require complex parameterization and it avoids the effects of uncertainty associated with parameterization. As a result, this paper chooses the GRO algorithm to deal with the microgrid optimization problem, and proposes targeted improvements to address the issues of poor convergence and an inclination to fall into local optima, aiming to better adapt to the complexity, dynamics, and high-reliability requirements of multi-energy scheduling in microgrid systems.

The contributions of this paper are as follows:

1. It establishes a CCHP microgrid optimization scheduling model based on the IGRO algorithm.
2. With the aim of addressing the shortcomings of poor convergence and susceptibility to becoming trapped in local optima, the initialization mechanism and search strategies of the algorithm are improved.
3. Several benchmark functions are employed for simulation and comparative analysis to verify the superior convergence accuracy of the proposed IGRO algorithm compared to other algorithms.
4. The IGRO algorithm is applied to optimize scheduling in a microgrid, demonstrating its effectiveness in addressing the scheduling optimization problem when compared to other algorithms.

2. Mathematical Model of CCHP System

Figure 1 shows the structure of the CCHP system. The electricity load is mainly met by the power grid, photovoltaics (PV), wind turbines (WT), and a gas turbine (GT). When electricity is abundant, excess power can be sold back to the grid. The heating load is met by the waste heat boiler (WHB), gas boiler (GB), and electric boiler (EB), while the cooling load is supplied by the absorption chiller (AC) and electric refrigeration (ER). Storage batteries (BT), thermal storage tanks (HS), and cold storage tanks (CS) play roles in supplying electricity, heating, and cooling loads, as well as in peak shaving.

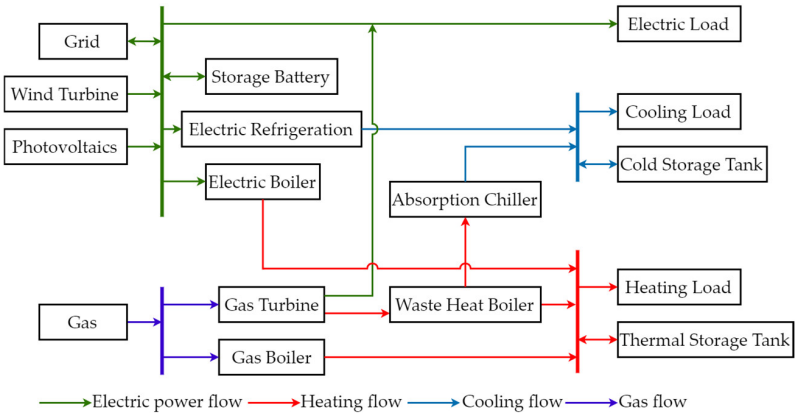

Figure 1. CCHP system structure diagram.

2.1. Mathematical Model of Gas Turbine

The gas turbine uses natural gas as fuel, and is capable of recovering waste heat to provide heating for users while generating electricity. The corresponding mathematical expressions are as follows [36]:

$$\begin{cases} P_{\mathrm{GT}}^{\mathrm{e}}(t) = \eta_{\mathrm{GT}}^{\mathrm{e}} P_{\mathrm{GT}}^{\mathrm{g}}(t), \\ P_{\mathrm{GT}}^{\mathrm{h}}(t) = \eta_{\mathrm{GT}}^{\mathrm{h}} P_{\mathrm{GT}}^{\mathrm{g}}(t). \end{cases} \tag{1}$$

In Equation (1), $P_{\mathrm{GT}}^{\mathrm{e}}(t)$, $P_{\mathrm{GT}}^{\mathrm{h}}(t)$, and $P_{\mathrm{GT}}^{\mathrm{g}}(t)$ are the output electric power, thermal power, and natural gas power consumed by the gas turbine in time period t, respectively; $\eta_{\mathrm{GT}}^{\mathrm{e}}$ and $\eta_{\mathrm{GT}}^{\mathrm{h}}$ are the efficiency of electricity production and heat generation of the gas turbine, respectively.

2.2. Mathematical Model of Gas Boiler

Natural gas is burned in the gas boiler to provide heat; the mathematical expression associated with this process is as follows:

$$P_{\mathrm{GB}}^{\mathrm{h}}(t) = \eta_{\mathrm{GB}} P_{\mathrm{GB}}^{\mathrm{g}}(t). \tag{2}$$

In Equation (2), $P_{\mathrm{GB}}^{\mathrm{h}}(t)$ and $P_{\mathrm{GB}}^{\mathrm{g}}(t)$ are the thermal power output and the natural gas power consumed by the gas boiler at time t, respectively; η_{GB} is the heat generation efficiency of the gas boiler.

2.3. Mathematical Model of Waste Heat Boiler

The waste heat boiler provides heat by absorbing waste heat from the exhaust gases produced by the gas turbine. The mathematical model is as follows:

$$P_{\mathrm{WHB}}^{\mathrm{h}}(t) = \eta_{\mathrm{WHB}} P_{\mathrm{GT}}^{\mathrm{h}}(t). \tag{3}$$

In Equation (3), $P_{\mathrm{WHB}}^{\mathrm{h}}(t)$ and η_{WHB} are the thermal power output and heat generation efficiency of the waste heat boiler at time t, respectively.

2.4. Mathematical Model of Electric Boiler

The electric boiler is a device that generates heat energy by flowing electrical energy through a high-resistance element; the mathematical expression is as follows:

$$P_{\mathrm{EB}}^{\mathrm{h}}(t) = \eta_{\mathrm{EB}} P_{\mathrm{EB}}^{\mathrm{e}}(t). \tag{4}$$

In Equation (4), $P_{\mathrm{EB}}^{\mathrm{h}}(t)$, $P_{\mathrm{EB}}^{\mathrm{e}}(t)$, and η_{EB} are the thermal power output, consumed electric power, and heat generation efficiency of the electric boiler at time t, respectively.

2.5. Mathematical Model of Electric Refrigeration

The electric refrigeration uses electric energy to drive compressors and transfer heat through refrigerant circulation to achieve refrigeration. The mathematical model is as follows:

$$P_{\mathrm{ER}}^{\mathrm{c}}(t) \;=\; \eta_{\mathrm{ER}} P_{\mathrm{ER}}^{\mathrm{e}}(t). \tag{5}$$

In Equation (5), $P_{\mathrm{ER}}^{\mathrm{c}}(t)$, $P_{\mathrm{ER}}^{\mathrm{e}}(t)$, and η_{ER} are the cooling power output, consumed electric power, and cooling efficiency of the electric refrigeration at time t, respectively.

2.6. Mathematical Model of Absorption Chiller

The absorption chiller is a device that drives refrigeration by absorbing thermal energy, and its mathematical model is as follows:

$$\begin{cases} P_{\mathrm{AC}}^{\mathrm{h}}(t) \;=\; \mu_{\mathrm{AC}} P_{\mathrm{WHB}}^{\mathrm{h}}(t), \\ P_{\mathrm{AC}}^{\mathrm{c}}(t) \;=\; \eta_{\mathrm{AC}} P_{\mathrm{AC}}^{\mathrm{h}}(t). \end{cases} \tag{6}$$

In Equation (6), $P_{\mathrm{AC}}^{\mathrm{c}}(t)$ and $P_{\mathrm{AC}}^{\mathrm{h}}(t)$ express the output cooling power and input heating power of the absorption chiller at time t, respectively; μ_{AC} is the proportion of heat delivered from the waste heat boiler to the absorption chiller; and η_{AC} is the cooling efficiency of the absorption chiller.

2.7. Mathematical Model of Energy Storage Devices

The energy storage devices include storage batteries, thermal storage tanks, and cold storage tanks. The corresponding mathematical expressions are as follows:

$$\begin{cases} P_s(t) \;=\; P_s^{\mathrm{cha}}(t)\eta_s^{\mathrm{cha}} - P_s^{\mathrm{dis}}(t)/\eta_s^{\mathrm{dis}}, \\ S_s(t) \;=\; S_s(t-1) + P_s(t), \\ 0 \le P_s^{\mathrm{cha}}(t) \le B_s^{\mathrm{cha}}(t) P_s^{\mathrm{cha,max}}, \\ 0 \le P_s^{\mathrm{dis}}(t) \le B_s^{\mathrm{dis}}(t) P_s^{\mathrm{dis,max}}, \\ S_s(0) \;=\; S_s(T), \\ B_s^{\mathrm{cha}}(t) + B_s^{\mathrm{dis}}(t) \le 1, \\ S_s^{\min} \le S_s(t) \le S_s^{\max}, \\ s \in \{\mathrm{BT}, \mathrm{HS}, \mathrm{CS}\}. \end{cases} \tag{7}$$

In Equation (7), s is the collection of electricity, heat, and cold energy storage; $P_s^{\mathrm{cha}}(t)$ and $P_s^{\mathrm{dis}}(t)$ are the energy storage device's charging and discharging powers during the time period t, respectively; η_s^{cha} and η_s^{dis} are the charging efficiency and discharging efficiency of the energy storage device, respectively; $S_s(t)$ and $S_s(t-1)$ are the capacities of energy storage devices at different time periods; $P_s^{\mathrm{cha,max}}$ and $P_s^{\mathrm{dis,max}}$ are the maximum power of single charging and discharging energy, respectively; $B_s^{\mathrm{cha}}(t)$ and $B_s^{\mathrm{dis}}(t)$ are binary variables representing the charging and discharging state parameters of the energy storage device during time period t, respectively; and $S_s^{\max}$ and $S_s^{\min}$ represent the upper and lower limits of the energy storage device's capacity.

2.8. Power Constraints

2.8.1. Constraints of Energy Balance

Energy balance includes electrical balance, thermal balance, and cold balance. The corresponding mathematical expressions are as follows:

$$P_{\mathrm{grid}}(t) + P_{\mathrm{WT}}(t) + P_{\mathrm{PV}}(t) + P_{\mathrm{BT}}^{\mathrm{dis}}(t) + P_{\mathrm{GT}}^{\mathrm{e}}(t) \;=\; P_{\mathrm{load}}^{\mathrm{e}}(t) + P_{\mathrm{BT}}^{\mathrm{cha}}(t) + P_{\mathrm{ER}}^{\mathrm{e}}(t) + P_{\mathrm{EB}}^{\mathrm{e}}(t). \tag{8}$$

$$P_{\mathrm{EB}}^{\mathrm{h}}(t) + P_{\mathrm{WHB}}^{\mathrm{h}}(t) - P_{\mathrm{AC}}^{\mathrm{h}}(t) + P_{\mathrm{GB}}^{\mathrm{h}}(t) + P_{\mathrm{HS}}^{\mathrm{dis}}(t) \;=\; P_{\mathrm{load}}^{\mathrm{h}}(t) + P_{\mathrm{HS}}^{\mathrm{cha}}(t). \tag{9}$$

$$P_{\mathrm{ER}}^{\mathrm{c}}(t) + P_{\mathrm{AC}}^{\mathrm{c}}(t) + P_{\mathrm{CS}}^{\mathrm{dis}}(t) \;=\; P_{\mathrm{load}}^{\mathrm{c}}(t) + P_{\mathrm{CS}}^{\mathrm{cha}}(t). \tag{10}$$

In Equations (8)–(10), $P_{\mathrm{load}}^{\mathrm{e}}(t)$, $P_{\mathrm{load}}^{\mathrm{h}}(t)$, and $P_{\mathrm{load}}^{\mathrm{c}}(t)$ are the electric load, heating load, and cooling load at time t, respectively.

2.8.2. Constraints of Power Grid

$$\left|P_{\mathrm{grid}}(t)\right| \le P_{\mathrm{grid}}^{\max}. \tag{11}$$

In Equation (11), $P_{\mathrm{grid}}(t)$ is the power of exchange with the grid in time period t, and $P_{\mathrm{grid}}^{\max}$ is the maximum power of purchasing or selling from the grid.

2.8.3. Constraints of Equipment

$$\begin{cases} 0 \le P_{\mathrm{GT}}^{\mathrm{e}}(t) \le P_{\mathrm{GT}}^{\mathrm{e,max}}, \\ 0 \le P_{GB}^{\mathrm{h}}(t) \le P_{\mathrm{GB}}^{\mathrm{h,max}}, \\ 0 \le P_{\mathrm{EB}}^{\mathrm{h}}(t) \le P_{\mathrm{EB}}^{\mathrm{h,max}}, \\ 0 \le P_{\mathrm{ER}}^{\mathrm{c}}(t) \le P_{\mathrm{ER}}^{\mathrm{c,max}}. \end{cases} \tag{12}$$

In Equation (12), $P_{\mathrm{GT}}^{\mathrm{e,max}}$, $P_{\mathrm{GB}}^{\mathrm{h,max}}$, $P_{\mathrm{EB}}^{\mathrm{h,max}}$, and $P_{\mathrm{ER}}^{\mathrm{c,max}}$ are the maximum output power of GT, GB, EB, and ER.

2.9. Objective Function

This paper optimizes the output of controllable devices with the goal of minimizing the system's electricity purchase and sale cost, fuel cost, maintenance cost, and environmental cost.

$$F \;=\; \min \sum_{t=1}^{T} \left(C_G(t) + C_F(t) + C_M(t) + C_E(t)\right). \tag{13}$$

In Equation (13), $C_G(t)$, $C_F(t)$, $C_M(t)$, and $C_E(t)$ are the cost of purchasing and selling electricity, fuel cost, maintenance cost, and environmental cost, respectively. Their specific expressions are as follows:

$$C_G(t) \;=\; \begin{cases} P_{\mathrm{grid}}(t)c_{\mathrm{buy}}(t), & P_{\mathrm{grid}}(t) \ge 0, \\ P_{\mathrm{grid}}(t)c_{\mathrm{sell}}(t), & P_{\mathrm{grid}}(t) < 0. \end{cases} \tag{14}$$

$$C_F(t) \;=\; \frac{c_{\mathrm{gas}}}{L}\left(P_{\mathrm{GT}}^{\mathrm{g}}(t) + P_{\mathrm{GB}}^{\mathrm{g}}(t)\right). \tag{15}$$

$$C_M(t) \;=\; \sum_{i=1}^{n} K_i P_i(t). \tag{16}$$

$$C_E(t) \;=\; \sum_{k=1}^{3} \left(\lambda_{\mathrm{GT},k} P_{\mathrm{GT}}^{\mathrm{e}}(t) + \lambda_{\mathrm{GB},k} P_{\mathrm{GB}}^{\mathrm{h}}(t) + \lambda_{\mathrm{G},k} P_{\mathrm{G}}(t)\right) c_k. \tag{17}$$

In Equations (14)–(17), $c_{\mathrm{buy}}(t)$ and $c_{\mathrm{sell}}(t)$ are the prices of purchasing and selling one unit of electricity at time t, respectively; c_{gas} and L are the cost per unit of natural gas consumed by gas equipment and the low calorific value of natural gas, respectively; K_i is the unit maintenance cost of the ith piece of equipment; $P_i(t)$ is the power output or consumption of the ith device at time t; $\lambda_{\mathrm{GT},k}$, $\lambda_{\mathrm{GB},k}$, and $\lambda_{\mathrm{G},k}$ represent the emission factors for the kth pollutant from the gas turbine, the gas boiler, and the upper grid, respectively; $P_{\mathrm{G}}(t)$ is the power purchased from the upper grid during time period t; and c_k is the unit cost of treatment for the kth pollutant gas.

3. Improvements to the GRO Algorithm

In the GRO algorithm, gold miners search for gold in three main ways: migration, gold mining, and cooperation. These modes allow the GRO algorithm to balance local exploitation and global exploration, which improves the speed of convergence and the reliability of obtaining a globally optimal solution.

3.1. Gold Rush Algorithm

3.1.1. Migration of Prospectors

The migration model simulates the behavior of gold miners who congregate in a particular area after information about a gold mine spreads. When certain regions are found to contain large amounts of gold, gold miners will quickly migrate to these regions in the hope of harvesting more wealth. In the algorithm, this process is realized by migration to regions with the current optimal solution or a potentially better solution. Equations (18) and (19) model the migration of prospectors to gold mines:

$$D_1 = C_1 \cdot X^*(t) - X_i(t). \tag{18}$$

$$X_i(t+1) = X_i(t) + A_1 \cdot D_1. \tag{19}$$

where $X^*(t)$, $X_i(t)$, and $X_i(t+1)$ are the location of the best gold mine, the location of the gold prospector i, and the new location of the gold prospector i, respectively. A_1 and C_1 are the vector coefficients calculated from Equations (20) and (21):

$$A_1 = 1 + l_1\left(r_1 - \frac{1}{2}\right). \tag{20}$$

$$C_1 = 2r_2. \tag{21}$$

where r_1 and r_2 are random numbers with values in the range [0, 1]. l_1 is the convergence component defined by Equation (22); if e equals one, it declines linearly from 2 to $1/t_{\max}$, and for values greater than one, it decreases non-linearly.

$$l_e = \left(\frac{t_{\max} - t}{t_{\max} - 1}\right)^e \left(2 - \frac{1}{t_{\max}}\right) + \frac{1}{t_{\max}}. \tag{22}$$

3.1.2. Gold Mining

Each gold miner mines gold areas to find more gold. The relevant mathematical expressions for gold mining are as follows:

$$D_2 = X_i(t) - X_r(t). \tag{23}$$

$$X_i(t+1) = X_r(t) + A_2 \cdot D_2. \tag{24}$$

$$A_2 = 2l_2 r_1 - l_2. \tag{25}$$

where $X_r(t)$ is the position of a randomly chosen gold prospector.

3.1.3. Collaboration Between Prospectors

$$D_3 = X_{g2}(t) - X_{g1}(t). \tag{26}$$

$$X_i(t+1) = X_i(t) + r_1 \cdot D_3. \tag{27}$$

Equations (26) and (27) represent the cooperation between gold prospectors, where $X_{g1}(t)$ and $X_{g2}(t)$ are two randomly selected gold prospectors.

3.2. Improved Gold Rush Algorithm

3.2.1. Halton Sequence Initialization

Initialization is a crucial part of intelligent optimization algorithms. Traditional initialization methods usually rely on pseudo-random number generation, which is simple to implement and has strong randomness, but it may lead to uneven distribution of population individuals in the search space, thus missing a large number of potential search areas [37]. The technique based on reverse learning first generates the original population and then adjusts the ineligible individuals through reverse learning. Although this approach can achieve better results, its performance is still affected by the quality of the initial generated population, and additional computational resources are required for fitness evaluation. In addition, population initialization methods based on chaotic techniques are widely used in optimization algorithms, and studies have shown that populations generated from chaotic sequences can achieve better results compared to those generated from pseudo-random numbers. However, although this method is globally more stable, it is locally unstable and highly sensitive to initial conditions and parameter settings. Based on the above problems, the IGRO algorithm adopts a more advanced quasi-random sequence, the Halton sequence, to initialize the population; this is a kind of low-discrepancy, deterministic sequence based on the construction of primes, which can make the population more uniformly distributed in the solution space, enhance the diversity of the population, and thus improve the convergence speed and accuracy of the algorithm effectively.

Assuming that the search space is two-dimensional, the generation process of the Halton sequence is as follows: firstly, two prime numbers are selected as bases, corresponding to two dimensions. Then, in each dimension, the interval (0, 1) is repeatedly sliced and taken in a roundabout way according to the selected bases, so as to obtain a set of non-repeated and uniformly distributed points. The mathematical model of the slicing process is shown in Equations (28)–(30):

$$n = \sum_{i=0}^{m} \alpha_i p^i = \alpha_0 + \alpha_1 p^1 + \cdots + \alpha_m p^m. \tag{28}$$

$$\phi_p(n) = \sum_{i=0}^{m} \alpha_i p^{-i-1} = \alpha_0 p^{-1} + \alpha_1 p^{-2} + \cdots + \alpha_m p^{-m-1}. \tag{29}$$

$$H(n) = \left[\phi_{p_1}(n), \phi_{p_2}(n)\right]. \tag{30}$$

where n denotes the ordinal number of the Halton sequence; p denotes the base of the Halton sequence, which takes the value of a prime number greater than or equal to 2; $\alpha_i \in \{0, 1, 2, \ldots p-1\}$, and it represents the digit expansion of n in base p; $\phi_{p_1}(n)$ and $\phi_{p_2}(n)$ are the defined sequence functions; and $H(n)$ is a two-dimensional uniform Halton sequence.

In two-dimensional space, assuming that the population size is 100 and the lower and upper bounds of the search space are 0 and 1, respectively, a comparison of the population distributions of random initialization and Halton sequence initialization is shown in Figure 2, where the bases of the Halton sequence are set as base1 = 2 and base2 = 3, respectively. It can be seen through the comparison that the population distribution of Halton sequence initialization is more uniform, which improves the diversity of the distribution of gold miners and thus helps to improve the performance of the algorithm.

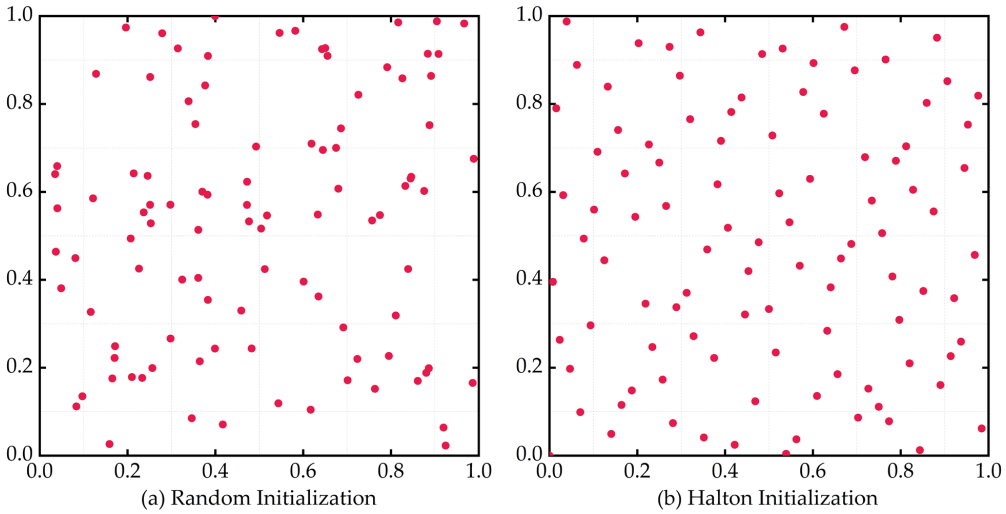

Figure 2. Random initialization and Halton initialization of gold miner distribution spaces.

3.2.2. Dynamic Adaptive Weighting Factor

In the particle swarm algorithm, inertia weights are one of the key parameters. Larger inertia weights facilitate a broader exploration of the search space, whereas smaller inertia weights contribute to more precise local exploitation. To enhance both the global exploration capability and the local search accuracy of the gold miners during the gold mining phase of the GRO algorithm, this paper introduces an adaptive weight factor based on iterative dynamic adjustment. The mathematical formulation of the adaptive weight factor is provided in Equation (31). In the early stage of iteration, as the location of the gold mine is still unclear, a larger weight factor helps the algorithm to conduct an extensive search to explore more possible solutions. In the late stage of iteration, as the location of the gold mine is gradually clarified, the space of the solution is gradually narrowed down, and during this time, a smaller weight factor allows the algorithm to focus on finer localized regions, thus improving its search efficiency and accuracy. By adjusting the size of the weighting factor, this method skillfully balances the search needs of the GRO algorithm at different stages, effectively improving the adaptability and accuracy of the algorithm in the multi-stage search process.

$$\omega = \exp\left(-(t/t_{\max})^2\right). \tag{31}$$

After introducing the dynamic adaptive weighting factor, the search path in the gold mining phase of the GRO algorithm is updated from Equation (24) to Equation (32):

$$X_i(t+1) = X_r(t) + \omega \cdot A_2 \cdot D_2. \tag{32}$$

3.2.3. Weighted Global Optimal Solution

In the GRO algorithm, the cooperative phase relies only on the distance between two randomly selected agents for position updating. Although this strategy possesses certain exploration capabilities across the entire search space, when dealing with optimization problems featuring a complex structure or multiple peaks, the search process tends to converge to local optima due to the absence of an effective global guidance mechanism, thereby limiting the algorithm's global optimization capability. For this reason, a weighted global optimal solution update strategy is introduced in the cooperation phase, as shown in Equations (33)–(36):

$$m = 1/(1+\exp(-20(t/t_{\max} - 0.5))). \tag{33}$$

$$D_4 = m \cdot (X^*(t) - X_i(t)). \tag{34}$$

$$D_5 = (1-m)\cdot(X_{g2}(t) - X_{g1}(t)). \tag{35}$$

$$X_i(t+1) = X_i(t) + r_1 \cdot (D_4 + D_5). \tag{36}$$

where m is a dynamically varying weight coefficient based on the sigmoid function, and its iterative value is shown in Figure 3. The value of m gradually increases with the number of iterations, indicating that the algorithm is more inclined to rely on random cooperation for extensive exploration in the early stage, while gradually enhancing the dominant role of the global optimal solution in the search process during the later stage, thus guiding the algorithm to smoothly transition from the random search in the early stage to the refined convergence process in the later stage. This strategy not only enhances the global search capability, but also maintains a certain local search capability by weighting the global optimal solution for location updating.

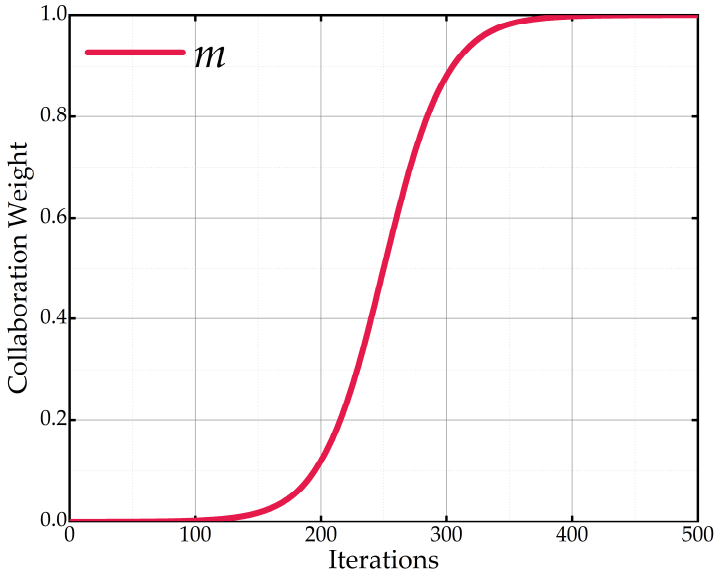

Figure 3. Collaborative weight values by number of iterations.

3.2.4. *t*-Distribution Mutation Strategy

Finally, a *t*-distribution mutation strategy is introduced to perturb the position of the optimal solution. This strategy combines the advantages of both Cauchy and Gaussian mutations, enhancing the global search capability in the early stages of the algorithm to avoid it becoming trapped in local optima, while in the later stages, it exhibits a stronger local exploitation ability, facilitating a more detailed exploration of the neighborhood around the optimal solution, and thereby effectively improving the convergence speed and accuracy of the algorithm. The specific expression is as follows:

$$\hat{X}^* = X^*\left(1 + \widehat{t}\,(t)\right). \tag{37}$$

where $\widehat{t}\,(t)$ denotes the *t*-distribution, whose degrees of freedom are determined by the number of iterations of the algorithm.

3.3. Implementation Process of IGRO Algorithm

A summary of the steps involved in the IGRO algorithm is shown in the flowchart in Figure 4.

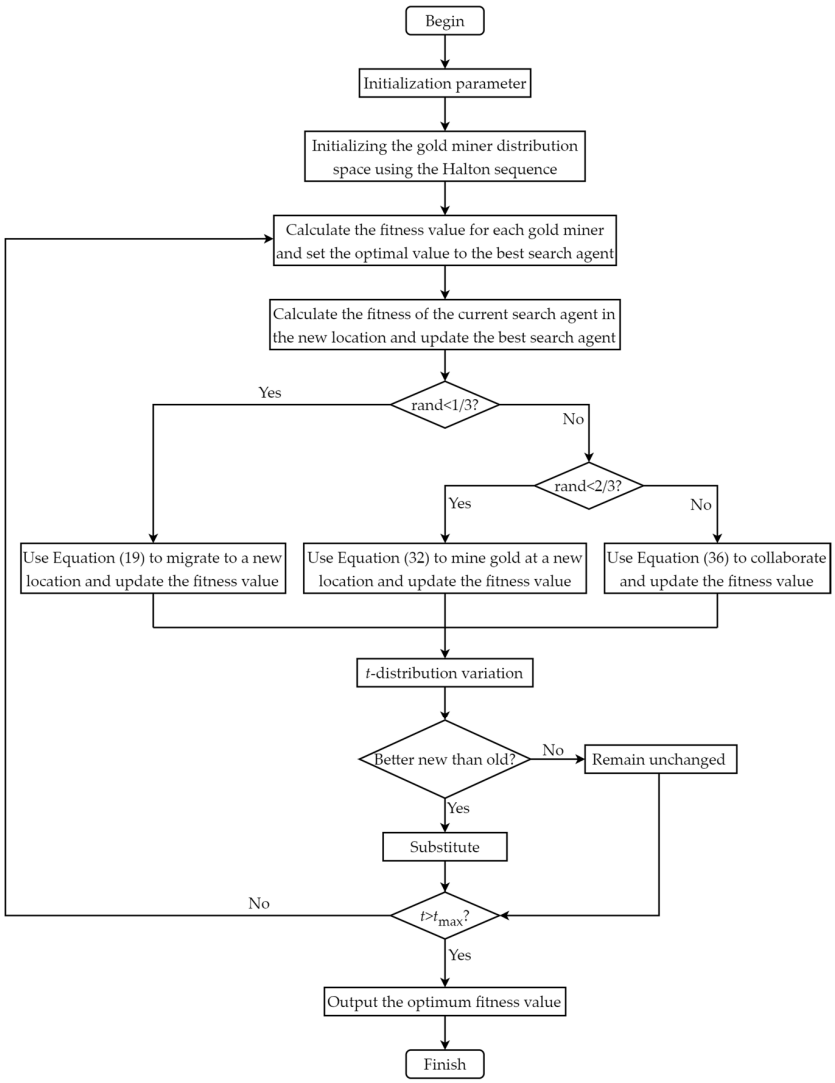

Figure 4. IGRO algorithm flowchart.

Step 1: Initialize the relevant parameters: gold miner size, dimensions, current number of iterations, maximum number of iterations, population search range, and convergence factor l_1, l_2;

Step 2: Initialize the gold miner population using the Halton sequence;

Step 3: Calculate the fitness value of each gold miner and set the optimal value X^* to the best search agent;

Step 4: Calculate the fitness of the current search agent at the new location and update the best search agent X^*;

Step 5: Use one of the methods among Equation (19)—migration, Equation (32)—gold mining, and Equation (36)—cooperation to calculate the new location of the search agent and update the fitness value;

Step 6: Update the optimal solution position using Equation (37);

Step 7: Determine whether the iteration termination condition is satisfied. If it is satisfied, then output the location of the gold prospector and its fitness value; otherwise, go to Step 3 to continue the execution.

3.4. Algorithm Performance Testing and Comparison

In order to verify the effectiveness of the IGRO algorithm, this study used 10 benchmark functions as test objects and solved the 10 benchmark functions using PSO [38],

WOA [39], GWO [40], HOA [41], and GRO, respectively. The names, definition domains, and theoretical optimal values of the test functions are shown in Table 1. Among them, F1–F4 are single-peak test functions, and F5–F10 are multi-peak test functions. The diversity of test functions can fully reflect the search performance of the IGRO algorithm.

Table 1. Basis functions.

Number	Names	Limitations	Reference Frame
F1	Sphere Function	[−100, 100]	0
F2	Schwefel's Problem 2.22	[−10, 10]	0
F3	Schwefel's Problem 1.2	[−100, 100]	0
F4	Quartic Function i.e., Noise	[−1.28, 1.28]	0
F5	Generalized Rastrigin's Function	[−5.12, 5.12]	0
F6	Ackley's Function	[−32, 32]	0
F7	Generalized Griewank's Function	[−600, 600]	0
F8	Generalized Penalized Function	[−50, 50]	0
F9	Shekel's Foxholes Function	[−65.54, 65.54]	0.998
F10	Kowalik's Function	[−5, 5]	0.0003

In order to avoid the effect of randomness, each algorithm was run 30 times and three metrics were used to measure the performance of the various algorithms: the optimal value, average value, and standard deviation. The resulting metrics of the functions are shown in Table 2. From Table 2 and Figure 5, it can be seen that the IGRO algorithm has significant advantages compared to the other algorithms when solving 10 benchmark test functions. Its optimal and average values are superior to those of the other algorithms, and the standard deviation is relatively small. For most of the test functions, the IGRO algorithm not only outperforms the other algorithms in terms of solution accuracy, but also exhibits faster convergence. Therefore, the overall performance of the IGRO algorithm is the best and most stable among the tested algorithms. In summary, the improved GRO algorithm shows significant advantages in convergence speed and accuracy, and these advantages make it more competitive than traditional algorithms in dealing with complex optimization problems.

Table 2. Test results of 6 types of intelligent algorithms for different benchmark functions.

Function	Metric	PSO	WOA	GWO	HOA	GRO	IGRO
F1	Best	1.12×10^{-5}	2.79×10^{-94}	7.84×10^{-35}	1.66×10^{-28}	2.73×10^{-78}	0
	Mean	2.78×10^{-4}	2.18×10^{-86}	2.07×10^{-33}	3.21×10^{-26}	1.02×10^{-72}	0
	Std	3.61×10^{-4}	8.42×10^{-86}	3.12×10^{-33}	6.10×10^{-26}	4.91×10^{-72}	0
F2	Best	2.60×10^{-4}	6.23×10^{-61}	6.76×10^{-21}	2.18×10^{-14}	6.33×10^{-48}	2.08×10^{-187}
	Mean	1.67	1.04×10^{-52}	7.81×10^{-20}	3.49×10^{-13}	1.43×10^{-45}	1.13×10^{-176}
	Std	3.79	4.08×10^{-52}	1.16×10^{-19}	3.35×10^{-13}	4.83×10^{-45}	1.71×10^{-177}
F3	Best	3.80×10^{2}	1.50×10^{4}	1.65×10^{-10}	2.54×10^{-23}	8.24×10^{-24}	0
	Mean	1.60×10^{3}	2.95×10^{4}	6.36×10^{-8}	1.39×10^{-21}	2.7	0
	Std	1.71×10^{3}	8.82×10^{3}	1.76×10^{-7}	2.21×10^{-21}	1.48×10	0
F4	Best	1.72×10^{-2}	1.05×10^{-4}	2.41×10^{-4}	4.87×10^{-5}	5.24×10^{-4}	1.13×10^{-6}
	Mean	3.45×10^{-2}	1.83×10^{-3}	1.16×10^{-3}	3.59×10^{-4}	4.15×10^{-3}	6.19×10^{-5}
	Std	1.12×10^{-2}	1.75×10^{-3}	5.69×10^{-4}	2.77×10^{-4}	2.94×10^{-3}	7.72×10^{-5}
F5	Best	2.39×10	0	0	0	0	0
	Mean	4.78×10	1.89×10^{-15}	1.03	1.45×10	0	0
	Std	1.24×10	1.04×10^{-14}	2.63	3.42×10	0	0

Table 2. *Cont.*

Function	Metric	PSO	WOA	GWO	HOA	GRO	IGRO
F6	Best	9.94×10^{-4}	8.88×10^{-16}	4.00×10^{-14}	1.51×10^{-14}	4.44×10^{-15}	8.88×10^{-16}
	Mean	1.03×10^{-1}	4.68×10^{-15}	4.30×10^{-14}	8.92×10^{-14}	4.68×10^{-15}	8.88×10^{-16}
	Std	3.59×10^{-1}	2.27×10^{-15}	3.82×10^{-15}	7.58×10^{-14}	9.01×10^{-16}	0
F7	Best	9.07×10^{-5}	0	0	0	0	0
	Mean	2.26×10^{-2}	2.61×10^{-3}	3.84×10^{-3}	0	0	0
	Std	2.90×10^{-2}	1.43×10^{-2}	6.90×10^{-3}	0	0	0
F8	Best	1.43×10^{-4}	1.37×10^{-3}	5.82×10^{-3}	2.94×10^{-1}	8.19×10^{-5}	2.79×10^{-5}
	Mean	2.04×10^{-1}	1.68×10^{-2}	2.76×10^{-2}	5.07×10^{-1}	7.09×10^{-4}	4.68×10^{-4}
	Std	2.90×10^{-1}	3.13×10^{-2}	1.53×10^{-2}	1.10×10^{-1}	1.02×10^{-3}	4.61×10^{-4}
F9	Best	9.98×10^{-1}	9.98×10^{-1}	9.98×10^{-1}	9.98×10^{-1}	9.98×10^{-1}	9.98×10^{-1}
	Mean	9.98×10^{-1}	1.72	2.45	2.93	1.06	9.98×10^{-1}
	Std	0	1.99	1.83	1.91	3.62×10^{-1}	0
F10	Best	3.07×10^{-4}	3.12×10^{-4}	3.07×10^{-4}	3.08×10^{-4}	3.07×10^{-4}	3.07×10^{-4}
	Mean	1.16×10^{-3}	5.56×10^{-4}	2.35×10^{-3}	3.43×10^{-4}	3.20×10^{-4}	3.18×10^{-4}
	Std	3.64×10^{-3}	2.81×10^{-4}	6.11×10^{-3}	5.85×10^{-5}	3.68×10^{-5}	3.14×10^{-5}

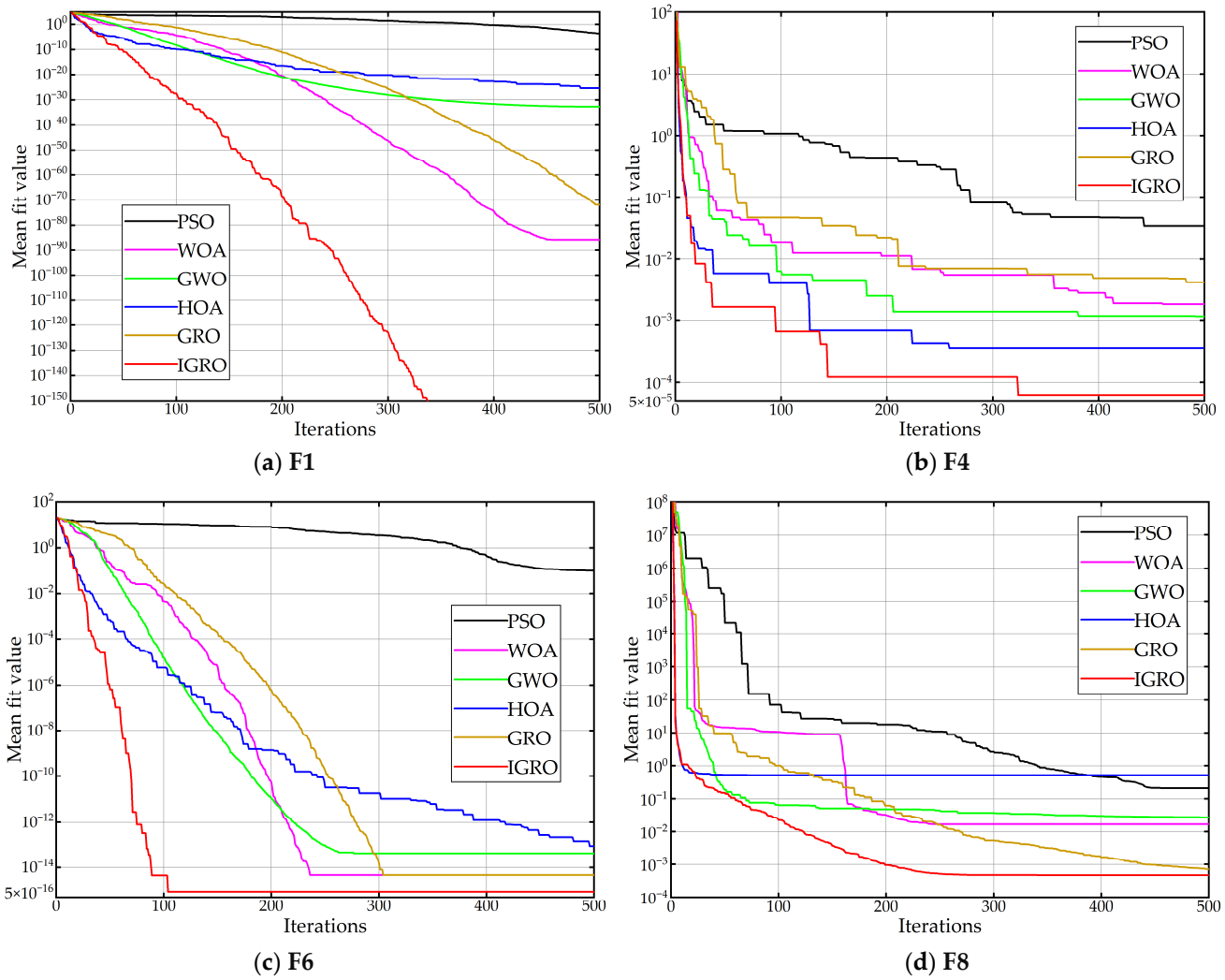

Figure 5. Convergence curves of selected test functions.

4. Calculus Analysis

4.1. Basic Parameter Settings of Microgrid

The time-of-use electricity price parameters are shown in Table 3 [42]. The emission factors and treatment cost parameters of the pollutant gases generated by the combustion of natural gas and the purchase of electricity are shown in Table 4, the maintenance parameters of each piece of equipment are shown in Table 5, and the typical daily load and predicted power of WT and PV are shown in Figure 6.

Table 3. Microgrid time-of-use electricity prices.

Periods	Purchase Price (¥/kWh)	Sale Price (¥/kWh)
Off-Peak Hours (0:00–7:00, 23:00–24:00)	0.1599	0.1230
Flat Hours (7:00–10:00, 15:00–18:00, 21:00–23:00)	0.4551	0.3567
Peak Hours (10:00–15:00, 18:00–21:00)	0.7749	0.6150

Table 4. Pollutant emission parameters.

Pollutant Types	Pollutant Emission Factors (g/kWh)			Treatment Costs (¥/kg)
	GT	GB	Grid	
CO_2	386	254	562	0.21
SO_2	0.0036	0.764	1.34	14.84
NO_x	0.2	0.54	1.47	62.96

Table 5. Equipment maintenance parameters.

Equipment	Price (¥/kW)	Equipment	Price (¥/kW)
WT	0.043	WHB	0.002
PV	0.029	AC	0.02
GT	0.15	ER	0.03
GB	0.15	EB	0.02
BT	0.016	HS	0.006
CS	0.008		

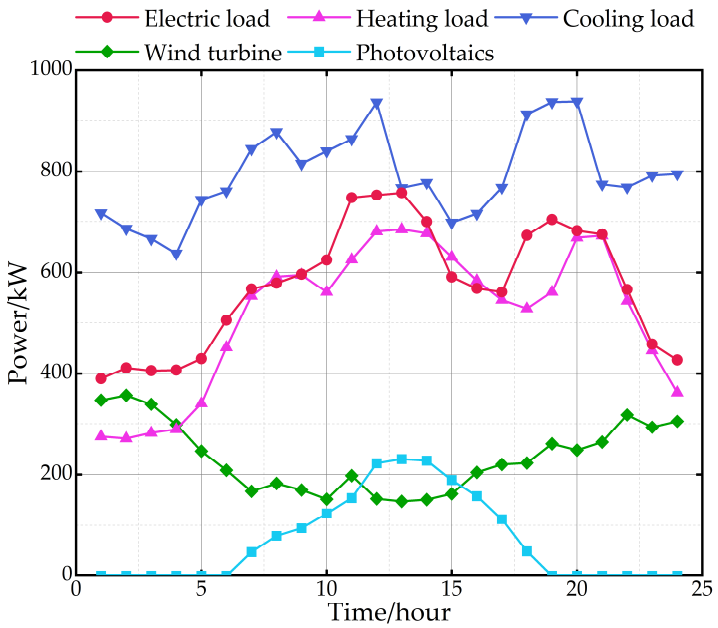

Figure 6. Typical daily load and predicted power of PV and WT.

4.2. Analysis of Simulation Results

Figures 7–9 show the optimal scheduling results for electrical, thermal, and cooling energy on a typical day of microgrid operation. In Figure 7, the gas turbine generates a significant share of the electricity, while the battery storage system is controlled to charge and discharge at different time intervals to support the power supply. During the nighttime hours between 1:00 and 4:00, the storage batteries switch to charging mode due to the low power demand, while electricity is purchased from the grid to meet the requirements of other electrical equipment. During periods of peak electricity demand, the batteries discharge stored energy to effectively alleviate pressure on the power grid, while also selling surplus electricity back to the grid to maximize economic returns. The electric boiler and the electric refrigeration consume electricity to meet the heating and cooling loads of the system, thereby contributing to stable and efficient energy system operation. From 7:00 to 9:00, since the heating cost of the gas boiler is higher than the revenue from selling electricity, the electric boiler consumes some of the electrical energy to produce heat. From 15:00 to 17:00, the storage batteries store surplus electricity to be discharged during the next period of peak electricity demand.

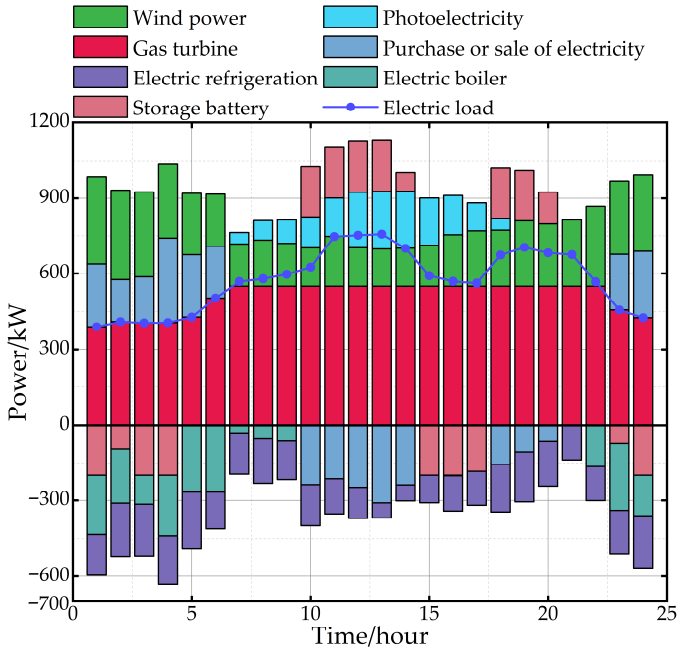

Figure 7. Electric power balance diagram.

In Figure 8, the waste heat boiler serves as the primary heat source for the microgrid. It recovers thermal energy from the high-temperature exhaust gas emitted by the gas turbine, meeting the majority of the system's heating load. The electric boiler and gas boiler adopt a time-of-use complementary operation strategy based on electricity price fluctuations. The electric boiler increases its output during low-electricity-price periods, while the gas boiler ramps up output during relatively high-electricity-price periods, thereby effectively reducing system operating costs. This time-of-use complementary operation strategy not only adheres to pricing standards, but also significantly extends the service life of the equipment. The thermal storage tanks store thermal energy during periods of low load and discharge it during peak heating demand in order to stabilize the heat supply. In the system, the waste heat boiler generates heat, part of which is used to meet the heating load, while the other part is absorbed by the absorption chiller to produce cooling. In Figure 9, the electric refrigeration reduces its output during periods of high electricity prices to maximize electricity sale revenue. The absorption chiller utilizes thermal energy to

drive the refrigeration cycle, effectively providing the required cooling load for the system. The stable operation of both the electric refrigeration and the absorption chiller ensures a steady cooling supply. The cold storage tanks accumulate cooling capacity during low-load periods and discharge it during peak cooling demand to serve as an auxiliary source. This strategy helps to regulate the load and mitigates the operational burden on the refrigeration system under high-load conditions.

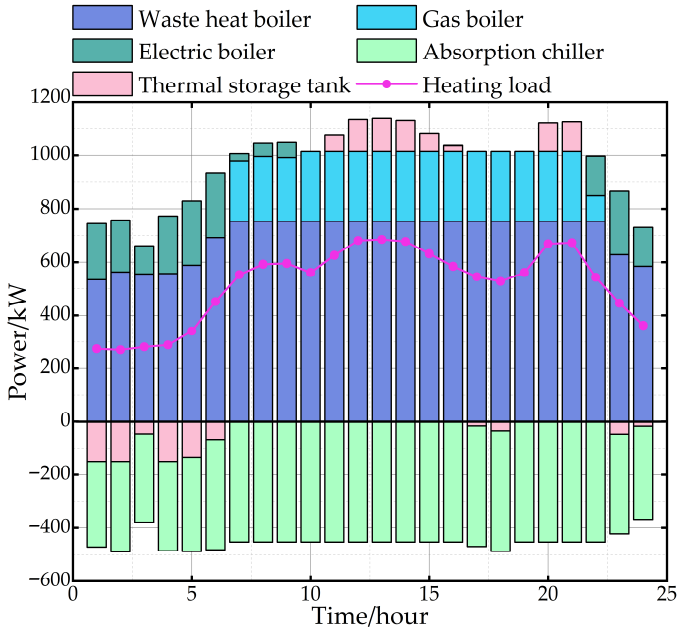

Figure 8. Thermal power balance diagram.

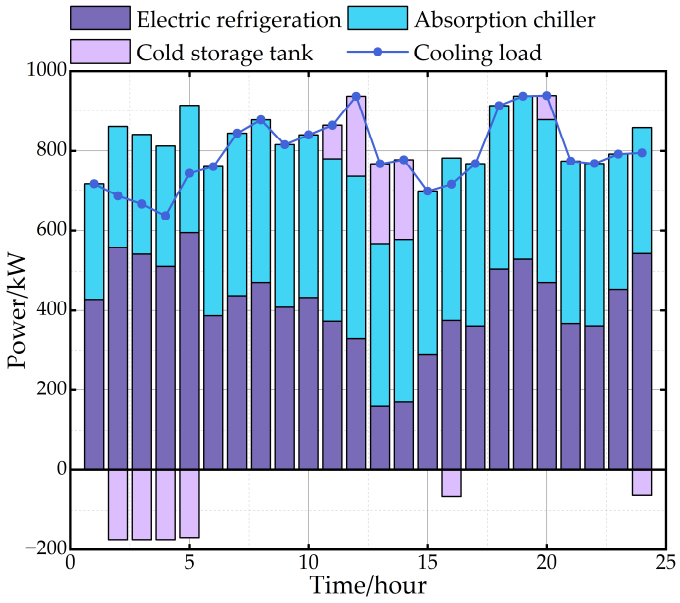

Figure 9. Cold power balance diagram.

To evaluate the stability and optimization capability of the IGRO algorithm, its performance on the microgrid case study proposed in this paper was benchmarked against that of the other algorithms, with each algorithm run independently 30 times. After 500 iterations, the obtained cost change curves are shown in Figure 10, while Table 6 presents the mean, standard deviation, optimal, and worst values for each algorithm, and Table 7 shows a comparison of the convergence time for each algorithm.

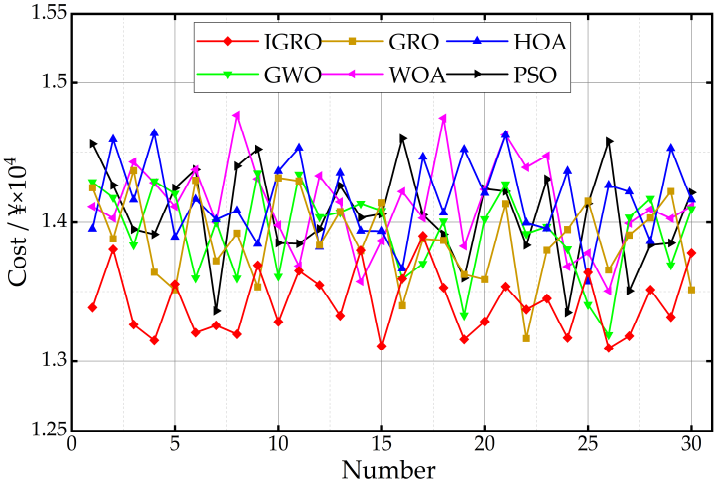

Figure 10. Comparison curve of daily microgrid operating costs obtained with each algorithm.

Table 6. Comparison of algorithmic results.

Algorithm	Daily Operation Cost of Microgrid (¥)			
	Average Value	Standard Deviation	Optimal Value	Worst Value
PSO	14,062.8	332.3	13,352.0	14,601.5
WOA	14,125.9	314.2	13,505.4	14,768.4
GWO	13,929.0	306.6	13,193.0	14,352.9
HOA	14,160.4	287.0	13,571.8	14,638.9
GRO	13,883.9	302.0	13,167.5	14,371.3
IGRO	13,426.9	230.1	13,096.3	13,904.3

Table 7. Comparison of convergence time.

Algorithm	PSO	WOA	GWO	HOA	GRO	IGRO
Convergence Time/s	282.3	327.5	278.3	265.4	293.8	275.5

From the algorithm comparison curve shown in Figure 10, it can be seen that the IGRO algorithm achieves the optimal scheduling scheme with the lowest economic cost, and the fluctuation of its curve is significantly smaller than that for the other algorithms in solving the problem of optimal microgrid scheduling. Base on analysis of the data in Table 6, the average cost value obtained with the IGRO algorithm is 3.29%, 5.18%, 3.60%, 4.95%, and 4.52% lower than that obtained with GRO, HOA, GWO, WOA, and PSO, respectively, and the standard deviation is 23.79%, 19.83%, 24.94%, 26.76% and 30.76% lower than that for other algorithms. At the same time, the optimal cost value obtained with the IGRO algorithm is better than the optimal value obtained with the other algorithms. As can be seen from Table 7, the IGRO algorithm demonstrates a shorter convergence time compared to the GRO algorithm, indicating a clear advantage in optimization efficiency. The above data show that the IGRO algorithm shows good stability and accurate optimization ability in solving the microgrid optimization problem.

5. Conclusions

This paper proposes an improved gold rush optimization algorithm to address the issues of poor convergence and the tendency to become trapped in local optima. By introducing Halton sequence initialization, a dynamic weight adjustment mechanism, a

weighted global optimal solution updating method, and a *t*-distribution mutation strategy, the proposed algorithm significantly enhances global search capabilities and accelerates convergence, while effectively reducing the risk of premature convergence caused by entrapment in local optima. To verify the effectiveness of the IGRO algorithm, 10 benchmark test functions were selected and simulation experiments were conducted with six intelligent algorithms. The experimental results demonstrate that the IGRO algorithm is significantly better than the other five algorithms in terms of search accuracy and convergence speed. In solving the problem of microgrid scheduling optimization, the IGRO algorithm exhibits lower operating costs and smaller standard deviations, indicating that the IGRO algorithm has high stability and application potential in microgrid optimization, further validating the feasibility and superiority of the algorithm.

Although the IGRO algorithm has demonstrated strong performance, this research still has certain limitations, due to the limited scope of study and computational constraints. Future research could focus on integrating dynamic adjustment mechanisms that adapt to different operating scenarios, making the algorithm's convergence time more flexible. This flexibility will make energy management more adaptable and efficient in response to changing environmental conditions and system loads. Furthermore, combining artificial intelligence with large-scale microgrids can further enhance the algorithm, improving optimization efficiency and scheduling accuracy. This integration of AI will enable better scalability and more robust performance in handling complex dynamic environments. Looking ahead, improving the algorithm's efficiency and broadening its applicability across diverse energy scenarios will be key to establishing it as a robust solution for the increasing demands and complexities of modern energy systems.

Author Contributions: Conceptualization, W.L. and Z.D.; methodology, W.L.; validation, W.L., Y.Y., and T.Z.; formal analysis, W.L.; investigation, W.L.; resources, W.L.; data curation, W.L.; writing—original draft preparation, W.L.; writing—review and editing, W.L.; visualization, W.L.; supervision, Z.D.; project administration, Z.D.; funding acquisition, J.C. All authors have read and agreed to the published version of the manuscript.

Funding: This research was funded by the National Natural Science Foundation of China under grant 52377110.

Data Availability Statement: The dataset is available on request from the authors.

Conflicts of Interest: The authors declare no conflicts of interest.

References

1. Zhou, X.Q.; Yu, W.L.; Ai, Q.; Zeng, S.Q. Review of optimal dispatch strategy of microgrid with CCHP system. *Electr. Power Autom. Equip.* **2017**, *37*, 26–33.
2. Gao, L.; Hwang, Y.; Cao, T. An overview of optimization technologies applied in combined cooling, heating and power systems. Renew. Sustain. *Energy Rev.* **2019**, *114*, 109344.
3. Azeem, O.; Ali, M.; Abbas, G.; Uzair, M.; Qahmash, A.; Algarni, A.; Hussain, M. A Comprehensive Review on Integration Challenges, Optimization Techniques and Control Strategies of Hybrid AC/DC Microgrid. *Appl. Sci.* **2021**, *11*, 6242. [CrossRef]
4. Dalala, Z.; Al-Omari, M.; Al-Addous, M.; Bdour, M.; Al-Khasawneh, Y.; Alkasrawi, M. Increased renewable energy penetration in national electrical grids constraints and solutions. *Energy* **2022**, *246*, 123361. [CrossRef]
5. Li, Y.; Wei, Y.; Zhu, F.; Du, J.; Zhao, Z.; Ouyang, M. The path enabling storage of renewable energy toward carbon neutralization in China. *Etransportation* **2023**, *16*, 100226. [CrossRef]
6. Liu, Y.; Dou, Z.; Wang, Z.; Guo, J.; Zhao, J.; Yin, W. Optimal Configuration of Electricity-Heat Integrated Energy Storage Supplier and Multi-Microgrid System Scheduling Strategy Considering Demand Response. *Energies* **2024**, *17*, 5436. [CrossRef]
7. Mahian, O.; Mirzaie, M.R.; Kasaeian, A.; Mousavi, S.H. Exergy analysis in combined heat and power systems: A review. *Energy Convers. Manag.* **2020**, *226*, 113467. [CrossRef]
8. Wang, S.X.; Zhu, W. Review on research of combined cooling heating and power microgrid planning. *Electr. Meas. Instrum.* **2021**, *58*, 10–17.

9. Wu, Q.; Han, J.; Jin, T.; Cai, C.; Meng, S.; Yin, J. Environmental and Economic Dispatch Model for Island Microgrid of Combined Cooling, Heating and Power. *Electr. Power* **2021**, *54*, 137–142.
10. Li, J.H.; Zhu, M.S.; Lu, Y.J.; Huang, Y.J.; Wu, T. Review on Optimal Scheduling of Integrated Energy Systems. *Power Syst. Technol.* **2021**, *45*, 2256–2272.
11. Gao, K.; Wang, T.; Han, C.; Xie, J.; Ma, Y.; Peng, R. A review of optimization of microgrid operation. *Energies* **2021**, *14*, 2842. [CrossRef]
12. Lei, B.; Ren, Y.; Luan, H.; Dong, R.; Wang, X.; Liao, J.; Fang, S.; Gao, K. A Review of Optimization for System Reliability of Microgrid. *Mathematics* **2023**, *11*, 822. [CrossRef]
13. Shezan, S.A.; Kamwa, I.; Ishraque, M.F.; Muyeen, S.; Hasan, K.N.; Saidur, R.; Rizvi, S.M.; Shafiullah, M.; Al-Sulaiman, F.A. Evaluation of different optimization techniques and control strategies of hybrid microgrid: A review. *Energies* **2023**, *16*, 1792. [CrossRef]
14. Wang, Z.; Dou, Z.; Dong, J.; Si, S.; Wang, C. Adaptive dynamic whale optimization algorithm with multi-strategy improvement. *Comput. Eng. Des.* **2022**, *43*, 2638–2645.
15. Li, Y.H.; Xian, R.C.; Zhang, H.Q.; Zhao, F.L.; Li, J.Y.; Wang, W.; Li, Z.Y. Fault Diagnosis for Power Transformers Based on Improved Grey Wolf Algorithm Coupled With Least Squares Support Vector Machine. *Power Syst. Technol.* **2023**, *47*, 1470–1478.
16. Du, X.; Hao, T.; Wang, B.; Wang, Z.; Zhang, J.; Jin, M. Artificial gorilla troops optimizer based on double random disturbance and its application of engineering problem. *J. Beijing Univ. Aeronaut. Astronaut.* **2025**, *51*, 1882–1896.
17. Wei, X.X.; Peng, M.S.; Huang, H.J. Node coverage optimization of wireless sensor network based on multi-strategy improved butterfly optimization algorithm. *J. Comput. Appl.* **2024**, *44*, 1009–1017.
18. Zhao, N.; Zhang, L.; Li, D.; Huang, W.; Xie, W.L.; Yang, Y.J. Optimal capacity allocation method for wind-solar-hydrogen-storage microgrid based on improved honey badger algorithm. *Electr. Eng.* **2025**, *20*, 338–351.
19. Peng, S.Q.; Guo, D.; Li, W.J.; Peng, H.Y.; Li, F. Parameter identification of PMSM based on improved mayfly algorithm. *Transducers Microsyst. Technol.* **2025**, *44*, 153–156+160.
20. Abd El-Sattar, H.; Hassan, M.H.; Vera, D.; Jurado, F.; Kamel, S. Maximizing hybrid microgrid system performance: A comparative analysis and optimization using a gradient pelican algorithm. *Renew. Energy* **2024**, *227*, 120480. [CrossRef]
21. Yuan, Z.; Wang, W.Q.; Wang, H.Y.; Khodaei, H. Improved butterfly optimization algorithm for CCHP driven by PEMFC. *Appl. Therm. Eng.* **2020**, *173*, 114766. [CrossRef]
22. Yun, B.; Bai, S.; Zhang, G. Optimization of CCHP system based on a chaos adaptive particle swarm optimization algorithm. *Power Syst. Prot. Control* **2020**, *48*, 123–130.
23. Li, J.; Wu, L.; Zhang, H.; Wang, W.; Jia, R. Microgrid economic dispatch of combined cooling, heating and power based on a rank pair learning crisscross optimization algorithm. *Power Syst. Prot. Control* **2021**, *49*, 137–145.
24. Fu, C.; Lin, K.; Zhou, Y. Optimal capacity configuration of CCHP system with improved operation strategies using improved multi-objective multi-universe algorithm. *Expert Syst. Appl.* **2022**, *199*, 117183. [CrossRef]
25. Zhao, Y.; Dou, Z.; Yu, Z.; Xie, R.; Qiao, M.; Wang, Y.; Liu, L. Study on the Optimal Dispatching Strategy of a Combined Cooling, Heating and Electric Power System Based on Demand Response. *Energies* **2022**, *15*, 3500. [CrossRef]
26. Qiao, M.; Yu, Z.; Dou, Z.; Wang, Y.; Zhao, Y.; Xie, R.; Liu, L. Study on Economic Dispatch of the Combined Cooling Heating and Power Microgrid Based on Improved Sparrow Search Algorithm. *Energies* **2022**, *15*, 5174. [CrossRef]
27. Si, S.; Dou, Z.; Wang, Z.; Dong, J. The analysis of time-sharing economic exergy efficiency of the CCHP system using planetary search algorithms. *J. Comput. Methods Sci. Eng.* **2023**, *23*, 2205–2224. [CrossRef]
28. Nan, J.; Xiao, Q.; Teimourian, M. Gas engine CCHP system optimization: An energy, exergy economic, and environment analysis and optimization based on developed northern goshawk optimization algorithm. *Heliyon* **2024**, *10*, e31208. [CrossRef]
29. Li, S.; Fang, X.; Liao, J.; Ghadamyari, M.; Khayatnezhad, M.; Ghadimi, N. Evaluating the efficiency of CCHP systems in Xinjiang Uygur Autonomous Region: An optimal strategy based on improved mother optimization algorithm. *Case Stud. Therm. Eng.* **2024**, *54*, 104005. [CrossRef]
30. Gao, Y.; Zhang, Y.; Xiong, Z.; Zhang, P.; Zhang, Q.; Jiang, W. Optimal scheduling model of microgrid based on improved dung beetle optimization algorithm. *Syst. Sci. Control Eng.* **2024**, *12*, 238533. [CrossRef]
31. Wang, Z.; Dou, Z.; Liu, Y.; Guo, J.; Zhao, J.; Yin, W. Research on Microgrid Optimal Scheduling Based on an Improved Honey Badger Algorithm. *Electronics* **2024**, *13*, 4491. [CrossRef]
32. Zolfi, K. Gold rush optimizer. A new population-based metaheuristic algorithm. *Oper. Res. Decis.* **2023**, *33*, 113–150. [CrossRef]
33. Kong, W.; Cai, X.; Du, Y.; Jia, B.; Zhang, X.; Wang, L.; Cheng, Z.; Shan, L. Wireless sensor network coverage optimization based on novel multi-strategy gold rush optimizer. *Electron. Lett.* **2024**, *60*, e13249. [CrossRef]
34. Lyu, L.X.; Kong, G.L.; Yang, F.; Li, L.; He, J. Augmented Gold Rush Optimizer Is Used for Engineering Optimization Design Problems and UAV Path Planning. *IEEE Access* **2024**, *12*, 134304–134339. [CrossRef]
35. Zong, Y.M.; Kong, W.B.; Li, J.P.; Wang, L.; Zhang, H.N.; Zhou, F.; Cheng, Z.Y. Optimization of Multilayer Microwave Absorbers using Multi-strategy Improved Gold Rush Optimizer. *Appl. Comput. Electromagn. Soc. J.* **2024**, *39*, 708–717. [CrossRef]

36. Chen, J.; Hu, Z.; Chen, Y.; Chen, J.; Chen, W.; Gao, M.; Lin, M.; Du, Y. Thermoelectric Optimization of Integrated Energy System Considering Ladder-Type Carbon Trading Mechanism and Electric Hydrogen Production. *Electr. Power Autom. Equip.* **2021**, *41*, 48–55.
37. Bangyal, W.H.; Rauf, H.T.; Batool, H.; Bangyal, S.A.; Ahmed, J.; Pervaiz, S. An improved particle swarm optimization algorithm with chi-square mutation strategy. *Int. J. Adv. Comput. Sci. Appl.* **2019**, *10*, 481–491. [CrossRef]
38. Kennedy, J.; Eberhart, R. Particle swarm optimization. In Proceedings of the ICNN'95-International Conference on Neural Networks, Perth, WA, Australia, 27 November–1 December 1995; Volume 4, pp. 1942–1948.
39. Mirjalili, S.; Lewis, A. The whale optimization algorithm. *Adv. Eng. Softw.* **2016**, *95*, 51–67. [CrossRef]
40. Mirjalili, S.; Mirjalili, S.M.; Lewis, A. Grey wolf optimizer. *Adv. Eng. Softw.* **2014**, *69*, 46–61. [CrossRef]
41. Oladejo, S.O.; Ekwe, S.O.; Mirjalili, S. The Hiking Optimization Algorithm: A novel human-based metaheuristic approach. *Knowl.-Based Syst.* **2024**, *296*, 111880. [CrossRef]
42. Xue, H. Economic Coordination of Microgrid with Renewable Energy Multi-objective optimization scheduling method. *Electrotech. Appl.* **2015**, *11*, 114–119.